IOPscience iopscience.iop.org

Home Search Collections Journals About Contact us My IOPscience

Point defects and stacking faults in $TiSi_2$ phases by tight binding molecular dynamics

This article has been downloaded from IOPscience. Please scroll down to see the full text article.

2002 J. Phys.: Condens. Matter 14 9535

(http://iopscience.iop.org/0953-8984/14/41/310)

View the table of contents for this issue, or go to the journal homepage for more

Download details:
IP Address: 171.66.16.96
The article was downloaded on 18/05/2010 at 15:09

Please note that terms and conditions apply.

J. Phys.: Condens. Matter **14** (2002) 9535–9553 PII: S0953-8984(02)39678-4

Point defects and stacking faults in $TiSi_2$ phases by tight binding molecular dynamics

M Iannuzzi[1]**, P Raiteri**[2]**, M Celino**[3] **and L Miglio**[2]

[1] CSCS, Swiss Center for Scientific Computing, via Cantonale, CH-6928 Manno, Switzerland
[2] INFM and Dipartimento di Scienza dei Materiali, Universitá degli Studi di Milano-Bicocca, Via Cozzi 53, I–20125, Milano, Italy
[3] ENEA 'Casaccia' Research Center, HPCN Project, CP2400-00100 Roma AD, Italy

E-mail: leo.miglio@unimib.it

Received 18 July 2002
Published 4 October 2002
Online at stacks.iop.org/JPhysCM/14/9535

Abstract
Tight binding molecular dynamics is used to predict the structure and the total energy of the most relevant intrinsic point defects in C54 and C49 $TiSi_2$. The comparison between the relative formation energies of point defects of the two phases in contact with a Si substrate suggests that the metastable C49 form has a higher concentration of point defects. In particular, we point out that Si vacancies and (010) stacking faults should be quite common in the C49 structure. This issue could be important in explaining the kinetic advantage of the latter phase in film growth by solid state reaction.

1. Introduction

This paper has its origin in our previous publication about the structural properties of bulk $TiSi_2$ phases [1]. There we introduced an original tight binding (TB) potential for $TiSi_2$ and a molecular dynamics code, which allow for the investigation of crystalline and amorphous phases in different thermodynamic conditions. In [1] we addressed the structural, electronic and thermoelastic properties of the two competitive phases (C54 and C49), along with the comparison to the amorphous phase, obtained by a temperature quenching of the simulated liquid phase. We concluded that the C49 phase displays smaller elastic parameters, i.e. it is mechanically softer with respect to the C54 one. In fact, the higher symmetry of the C54 lattice guarantees a very efficient overlap of the Ti d and Si p states, whereas the C49 phase is

0953-8984/02/419535+19$30.00 © 2002 IOP Publishing Ltd Printed in the UK

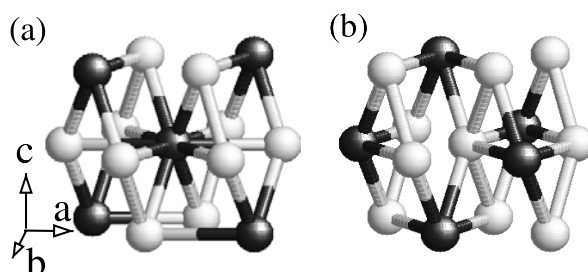

Figure 1. (a) First and second nearest neighbours in the C54 structure (within 4 Å) around Ti (black spheres); (b) the same for Si (light spheres).

more open and lower in symmetry, providing some Ti d non-bonding states [1][4,5]. It would be interesting to know if such a difference gives rise to different formation energy for some prototypical lattice defects. Actually, $TiSi_2$ is commonly applied in integrated circuits for local interconnects, gate metallization and Schottky barriers [2, 3], but very little is known about the intrinsic defects in the C54 and, particularly, in the C49 precursor phase. It is usually assumed that the C49 form is a metastable phase, which is kinetically favoured in the solid state reaction between a thin Ti overlayer and a Si substrate. The growth of the C49 phase proceeds by Si diffusion through the initial silicide layer [4, 5] until the Ti overlayer is exhausted, providing a metallic silicide with small lattice misfit with the Si substrate. In order to achieve the low resistivity C54 phase, a structural transition is thermally activated above 700 °C [6, 7]. Taking into account the diffusion-driven formation process of $TiSi_2$, it is likely that vacancies and interstitials are an important factor, but the precise estimation of the formation energies for such a compound material in contact with a Si reservoir is not a trivial matter. Actually, a relative comparison of the formation energies of point defects for the two phases would be sufficient, since a sizeable difference would imply a slight stoichiometric rebalancing during the phase transition from C49 to C54 $TiSi_2$. Another open question is the high density of SFs along the C49 [010] direction [8] and its relation to the scattered estimations of the corresponding lattice constant in such an orthorhombic phase [9, 10]. This issue is also very important in understanding the higher resistivity of the C49 phase [11]. Still, the actual structure and the experimental formation energy of the SFs are not known. This paper is the first attempt to provide a quantitative estimation for the formation energy of both point and extended defects, on the basis of one reliable interatomic potential.

2. Some remarks on the system and on our method

C49 and C54 $TiSi_2$ display orthorhombic unit cells containing two formula units (fu) per Bravais site: $a = 3.62$ Å, $b = 13.76$ Å, $c = 3.60$ Å for the C49 [12], and $a = 8.269$ Å, $b = 4.798$ Å, $c = 8.553$ Å for the C54 [13] phase. The former is base centred, whereas the

[4] In the C49 structure the low point symmetry around Ti gives rise to a high non-bonding peak of Ti d states in the electronic density of states (DOS) (cf figure4 in [1]). However, a partial quench of the peak is achieved by the structural relaxation driven by molecular dynamics runs, at finite temperature. See also footnote 6.

[5] By performing NPT equilibrations of the ideal bulk structure for a simulation cell of 32 conventional orthorhombic cells ($\tilde{a} = 14.49$ Å, $\tilde{b} = 27.52$ Å and $\tilde{c} = 14.40$ Å), the sides evolve to $\tilde{a} = 14.22$ Å, $\tilde{b} = 26.80$ Å and $\tilde{c} = 15.10$ Å, splitting the initial degeneracy of a and c sides, with a negligible decrease in volume, from 14.94 Å atom to 14.90 Å atom. This small spurious effect is partially produced by the empirical TB potential, which overestimates the anisotropy in the xz plane (see footnote 4). Still, it is qualitatively meaningful to compare this result to the ones obtained for the stacking fault (SF) configurations, in order to reveal any trend towards tetragonalization.

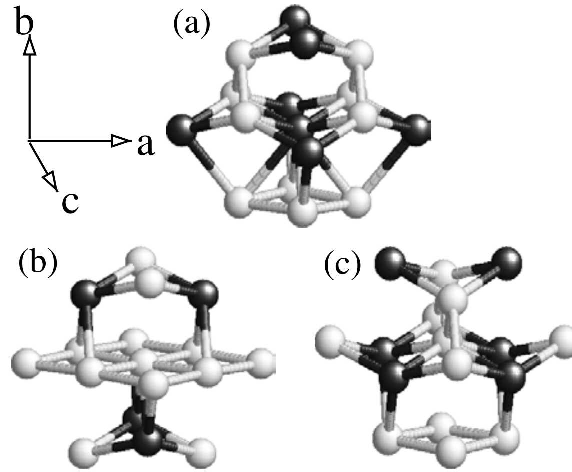

Figure 2. First and second nearest neighbours in the C49 structure (within 4 Å) around Ti (a), Si I (b) and Si II (c) sites in the C49 structure, as in figure 1.

Table 1. The site energy ξ_{tot} (our chemical potential) is given by the summation of the repulsive term ξ_{rep}, the TB bond energy term ξ_{bond} and the *onsite* term ξ_{onsite} (see the appendix). The two last columns display the numbers of Ti and Si first neighbours within 3 Å.

	Site	ξ_{rep} (eV)	ξ_{bond} (eV)	ξ_{onsite} (eV)	ξ_{tot} (eV)	Ti No of nn	Si No of nn
C54	Ti	9.69	−24.85	10.09	−5.07	0	10
	Si	7.98	−15.74	−1.61	−9.36	5	5
	Ti	8.97	−23.43	9.67	−4.72	0	10
C49	Si I	7.25	−14.39	−2.01	−8.97	4	4
	Si II	7.71	−16.00	−1.50	−9.75	6	2

latter is face centred. In both cases the first shell of neighbours around Ti contains ten Si atoms, between 2.53 and 2.80 Å (see table 1 and figures 1 and 2) [1]. However, the C49 structure has a lower symmetry than the C54 form and, in the former phase, the Si atoms are distributed into two inequivalent sub-lattices, where the sites are conventionally named Si I and Si II. Both of them are under-coordinated in the first shell of neighbours, but over-coordinated in the second shell, with respect to the C54 structure [1]. Figure 2 clearly shows that the Si I sites in the (010) plane are arranged in a square lattice (if the slight difference between the a and c lattice constants is neglected), where the Ti neighbours out of plane are quite far apart. Because of this square network, the electronic density of states projected onto the Si I layer is expected to display an sp-metal character, but not the one for a two-dimensional system, due to the presence of the neighbouring Ti planes. This is confirmed by the analysis of the low energy region of the projected DOS reported in figure 3 (middle panel), where the s and p contributions display a prototypical square-root behaviour, at variance with respect to the DOS projected on the Si II site in the C49 structure (bottom panel) and the Si site in the C54 case (top panel). This peculiarity is apparent also in the site energies, as calculated according to the appendix and reported in table 1. We see that the Si I sites display a lower covalent bonding with respect to the Si II sites and that the total site energy is higher by 1 eV.

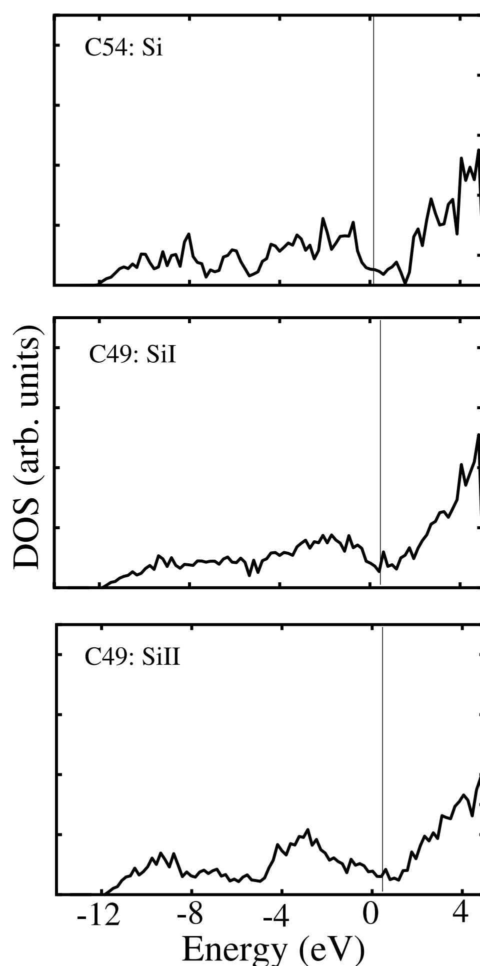

Figure 3. Site-projected electronic DOS in the C54 phase (top panel) and in the C49 phase. All the spectra refer to structures equilibrated by MD. The vertical line indicates the position of the Fermi level.

The strong point of the TB method, as well as other localized-base methods, is that a partitioning of the total energy into Ti, Si I and Si II contributions is possible and unique. The cohesion energy of the i-site can be in principle estimated as the difference between ξ^i_{tot} (the chemical potentials in our scheme, where the atomic cores are frozen) and ξ^i_{onsite} for the free atomic configuration, which is computed by summing the diagonal elements of the TB Hamiltonian[6] up to the number of valence electrons. The weak point of the orthogonal TB method, however, is that the diagonal elements of the Hamiltonian, i.e. the orbital energies, are fixed to the values fitted to reproduce at best the band diagram of the compound. Therefore, the energies of the atoms in vacuum are not only arbitrary with respect to an absolute scale (a rigid shift of the diagonal elements is here ineffective), but also do not account for the sizeable rearrangement of the orthogonalized orbitals when no overlap with the neighbours is present. This issue affects mostly the Ti atoms, displaying an energy gap between the Ti s and Ti d

[6] $E_s^{Si} = -4.00$ eV; $E_p^{Si} = 1.87$ eV; $E_d^{Ti} = 1.00$ eV; $E_s^{Ti} = 3.50$ eV; $E_p^{Ti} = 6.00$ eV. See also [1].

orbitals which is realistic just for bulk $TiSi_2$. For this reason, our estimated formation energy of $TiSi_2$ (19.29 eV per fu) is larger than the experimental value (15.44 eV per fu), as obtained by the formation energies of c-Si (450 kJ mol^{-1}) and c-Ti (473 kJ mol^{-1}) and C54 $TiSi_2$ from c-Si and c-Ti (171 kJ mol^{-1}) [14]. Because of such deficiencies the comparison of total energy configurations with different stoichiometries is not a trivial matter.

In our case, the estimation of defect formation energies in a compound material, such as vacancies and interstitials, would require the total energy calculation of defect pairs preserving the stoichiometry and the homogeneity of the system (Si precipitates counterbalancing Si vacancies, for instance). However, $TiSi_2$ phases grow as polycrystalline films on top of a Si substrate, and one Si vacancy is likely to correspond to one Si atom still in the Si substrate, whereas a Ti vacancy corresponds to two Si atoms which have moved to a $TiSi_2$ environment rather than staying in the Si substrate. Therefore, we understand that the key issue in this case is the estimation of the change in the Si chemical potential between crystalline silicon ($\xi_{tot}^{\mathrm{c-Si}}$) and $TiSi_2$ (ξ_{tot}^{Si}). As mentioned before, this is not an easy task, and only the difference between the formation energy of one particular point defect in the two $TiSi_2$ phases is quantitatively meaningful in TB calculations. In order to provide a hierarchy between Si vacancies, Si interstitials and Ti vacancies in one single phase, we note that $\xi_{tot}^{\mathrm{c-Si}}$ can be estimated, in our framework, by adding the experimental value of the c-Si formation energy per atom (−4.60 eV) to our reference energy ξ_{onsite}^{i} for Si in vacuum (−4.26 eV) (see footnote 7). The latter, at variance with Ti, is produced by $\Delta E_{\mathrm{s-p}} = 5.87$ eV, not far from the experimental value and well within the values usually adopted for a satisfactory estimation by TB approaches to silicon total energy calculations in different phases [15]. In this way, we believe that the difference in the chemical potential of Si inside $TiSi_2$ and c-Si can be consistently evaluated within our model to a better precision than the one provided by using the formation energy of c-Si obtained by rescaling our Si–Si hopping elements, which are optimized for a $TiSi_2$ environment [1].

3. Vacancies

The most common point defects in metallic and close-packed materials are vacancies. Experimental estimations of the vacancy concentration in the C54 and C49 phases of $TiSi_2$ are not available; nevertheless they are supposed to play a role in the growth of polycrystalline films by vacancy-assisted diffusion of silicon in the silicide [16]. In order to estimate the formation energy of Si and Ti vacancies, total energy calculations for one missing atom in the equilibrated supercell with three-dimensional periodic boundary conditions have been performed for both $TiSi_2$ phases. Reliable information is obtained only for supercell size such that no inter-cell defect interactions are present. Therefore, we performed a preliminary calculation for Ti and Si vacancies in the defected, still unrelaxed structures, by increasing the number of atoms: 191 (C54) or 215 (C49), 287, 383 and 575 atoms. Since satisfactory convergence in the formation energy to the second decimal digit (10^{-2} eV) was found for 383 atoms, molecular dynamics relaxation has been performed for such a cell size. The corresponding defect concentration is 1.81×10^{20} cm^{-3} in the C54 phase and 1.75×10^{20} cm^{-3} in the C49 phase[7].

The numerical preparation of the samples is the following. First we relax the perfect crystal structures at 1 K for 10 ps (the time step is 1 fs) by means of a molecular dynamics run at constant number of atoms, temperature and pressure (NPT). Then, the defect is created in

[7] In most of the calculations contained in this paper the atomic volumes of TiSi we refer to are the theoretical ones, obtained by MD equilibration for bulk C54 and C49 phases, as reported in [1]. In particular, $\Omega_0^{\mathrm{C54}} = 14.38$ Å^3 and $\Omega_0^{\mathrm{C49}} = 14.89$ Å^3 are one-third of the equilibrated volume per formula unit.

Table 2. Vacancy formation energies obtained by simulation cells containing 383 atoms plus one vacancy for NVT and NPT relaxation runs.

	Vacancy Site	NVT E_f (eV)	NPT E_f (eV)
C54	Ti	3.12	3.12
	Si	2.68	2.71
C49	Ti	1.83	1.85
	Si I	0.49	0.47
	Si II	1.89	1.86

a random site and the sample is heated up to 100 K in 2 ps, equilibrated for 2 ps or more and quenched back to 1 K in 4 ps (constant cooling rate 25 K ps^{-1}), either at constant pressure (NPT) or at constant volume (NVT). The time average of the total energy is collected by a further run at 1 K for 2 ps.

The formation energy for a Si vacancy is finally computed as

$$E_f^{\mathrm{Si}} = E^{\mathbb{N}-\mathrm{Si}} + \xi_{tot}^{\mathrm{c-Si}} - E^{\mathbb{N}}, \tag{1}$$

where $E^{\mathbb{N}-\mathrm{Si}}$ is the total energy of the sample containing the Si vacancy, $E^{\mathbb{N}}$ is the total energy of the original supercell with $\mathbb{N}$ fu and no defects, at 1 K, and $\xi_{tot}^{\mathrm{c-Si}}$ is the chemical potential for one Si atom still in the silicon substrate. The formation energy for a Ti vacancy is given by

$$E_f^{\mathrm{Ti}} = E^{\mathbb{N}-\mathrm{Ti}} + \xi_{tot}^{\mathrm{Ti}} + 2\xi_{tot}^{\mathrm{Si}} - 2\xi_{tot}^{\mathrm{c-Si}} - E^{\mathbb{N}} = E^{(\mathbb{N}+1)-\mathrm{Ti}} - 2\xi_{tot}^{\mathrm{c-Si}} - E^{\mathbb{N}}, \tag{2}$$

since it is understood that one Ti vacancy allows for the formation of one additional $\mathrm{TiSi_2}$ fu in place of two silicon atoms in the substrate. Here we did not consider the structural and energetic changes originated by Si vacancies in the substrate, since they are supposed to come from the interface region, which has moved a little bit farther.

In table 2 our formation energies are reported. By comparing the results for NVT and NPT relaxations we find no relevant differences. By the analysis of table 2 we see that E_f for Ti or Si vacancies is larger in the case of the C54 phase, which is a stiffer structure. This is probably determined by the fact that the orbital rebonding and the structural rearrangement around the vacancies propagate efficiently in the C49 structure.

Actually, in the TB model we can project the total energy on each atom (see the appendix) and compare the site energy before and after the relaxation. A picture of the distribution of the perturbation all over the cell is then obtained. In panels (a) and (b) of figures 4 and 5 (concerning the C54 sample and to the C49 sample, respectively) the site energy variations with respect to the corresponding unperturbed configuration are plotted with our conventional site index (Ti sites are the first 128 units). In panels (a) the perturbation at the first step (just the bond breaking) is represented, where only a few atoms close to the vacancy are affected by localized variation in energy. The peaks are positive when due to the breaking of the Ti–Si cohesive interaction. By contrast, the variations are mostly negative when they are caused by a Si–Si bond breaking, because of the lowering of their steric repulsion. Panels (b) show the final energy distribution, as computed after the NPT equilibration run. While in the C54 case (figure 4) the original peaks are only slightly reduced, the energy peaks corresponding to a Si vacancy in the C49 structure (figure 5) are drastically quenched, and a wide redistribution of the energy excess all over the simulation cell occurs.

The (c) panels of the same figures display the square displacement of each atom and confirm our hypothesis. When a Ti vacancy is created, the largest atomic change of position

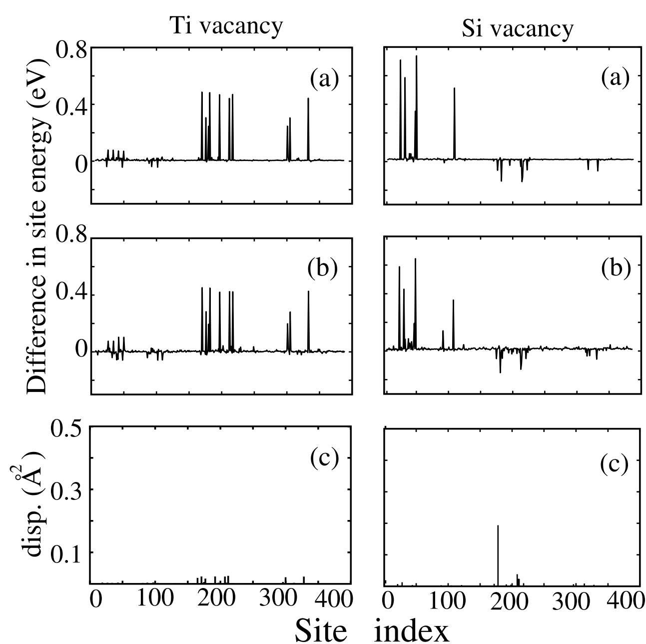

Figure 4. Energy and structural relaxation in the C54 supercell containing one vacancy versus site index (the first 128 units refer to Ti atoms). Left panels refer to the Ti vacancy; right ones to the Si vacancy. (a) Differences in site energies as the vacancy is created, (b) differences in site energies after the thermal annealing, (c) square displacements computed in the final atomic configuration with respect to the original one.

after the equilibration does not exceed few hundredths of an ångstrom, both in C54 and C49 structures. The case of the Si vacancy is different, since some Si neighbours are induced to move towards the vacancy by the absence of steric repulsion. This effect is likely to be produced also by the dangling bonds on the Ti atoms surrounding the vacancy site, which are saturated by rehybridization. In the C54 structure, only one Si atom significantly modifies its position (∼0.44 Å in the (001) plane), but the quasi-hexagonal configuration is preserved (figure 6).

In contrast, an extended relaxation occurs in the C49 phase, in particular for the Si I vacancy. In the latter case, one of the Si I neighbours lying in the xz plane (figure 7) ends up to an intermediate position between its original site and the vacancy. A simulated annealing above 600 K is sufficient to cause the hopping of the vacancy towards a neighbouring site, and a more symmetric configuration is obtained (figure 7, right panel). In the case of the Si II vacancy, the two nearest Si II atoms (figure 2 panel (c)) move parallel to the (100) plane, as indicated by the arrows in figure 8. However, their paths are considerably shorter than the ones for the case discussed above. Moreover, the first vacancy hopping along the Si II chain has been observed only at simulated annealing above 1000 K.

Our results in table 2 can also be interpreted on a quantitative scale, even if the formation energies calculated for a system composed by a $TiSi_2$ film plus the Si substrate do not allow a meaningful comparison to other calculations, such as the ones for TiAl [17], or measurements, such as the ones for Fe_3Si [18], which refer to a single bulk. What is clear is that the Si I vacancy in the C49 $TiSi_2$ displays a very small formation energy. Such an anomalous effect might be originated by the rather ‘metal-like’ bonding among the Si I atoms in the (010) layer, and with the Ti atoms above and below it (figure 2). In fact, as one Si I vacancy is created, the neighbour-

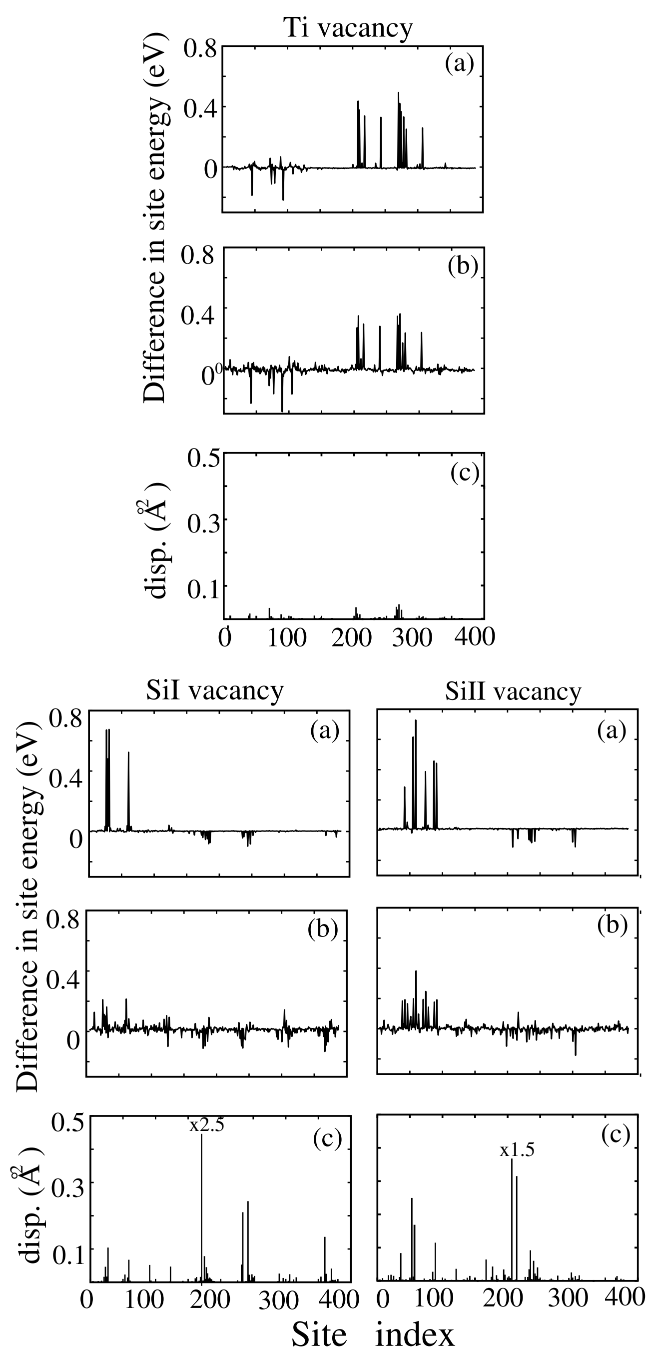

Figure 5. The same as in figure 4 for the C49 supercell containing one vacancy.

ing Si I atoms in the (010) plane readily move to fill the gap and the Ti–Si 'metal-like' bonding is partly restored at a lower steric repulsion. This is confirmed by the inspection of panels (b) and (c) in figure 5 and by the atomic displacements around the Si I vacancy, shown in figure 7.

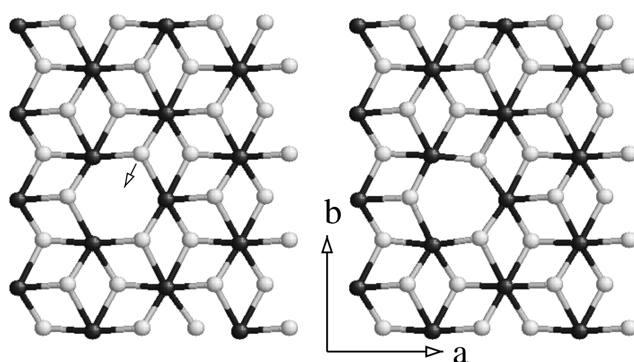

Figure 6. Plan view of the (001) plane containing one Si vacancy in the C54 structure, as it appears when the Si atom has just been extracted (left) and after the MD relaxation (right). The arrow indicates the largest atomic movement.

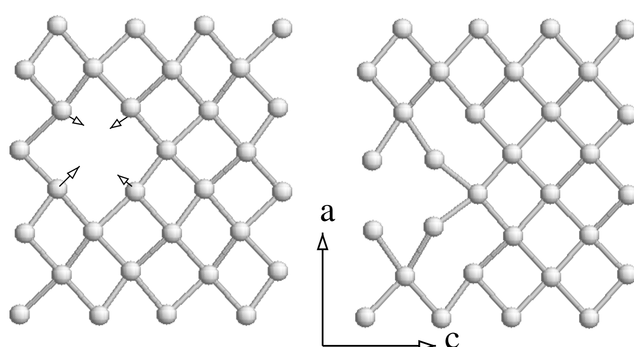

Figure 7. Plan view of the (001) plane containing one Si vacancy in the C49 structure, as it appears when the Si atom has just been extracted (left). The arrows indicate the atomic movements in the (010) plane with relaxation. After heating to 600 K a vacancy hopping and a more symmetric configuration is obtained (right).

More detailed information about the electronic effects due to the Si I vacancy may be recovered by the analysis of the DOS projected onto the neighbouring atoms. In particular, when a Ti vacancy is created in the C49 $TiSi_2$, only slight variations of the projected DOS are obtained. In contrast, the lack of a Si atom causes the formation of a peak, related to dangling bonds on the Ti neighbours, just above the Fermi level. This is particularly true for the C49 structure (see figure 9). Rebonding around the Si I vacancy is almost complete as the peak is quenched after the structural relaxation (left panel). However, in the case of the Si II vacancy, the peak is still present after the simulated annealing, even if slightly lowered as shown in the right panels of figure 9. We conclude that the dangling bond saturation has occurred to a smaller extent than in the previous case, somewhat similar to the case of the Si vacancy in the C54 phase (not shown here).

The vacancy equilibrium concentration is related to the formation energy and the formation entropy. By considering only the former, it is likely that, because of the small formation energy of Si I vacancies, the C49 structure is slightly substoichiometric with respect to the C54 form. This issue, if confirmed by some experimental indications, could partially explain the advantage of the C49 phase with respect to the C54 one in the early stages of the film growth, when substoichiometry in Si is likely to occur for kinetic reasons.

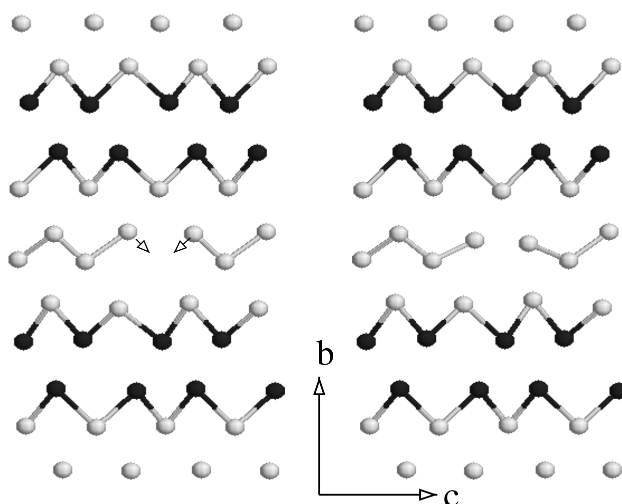

Figure 8. Plan view of the (100) plane containing one Si II vacancy in the C49 structure, as it appears when the Si II atom has just been extracted (left) and after the MD relaxation (right). The arrows point out the relevant atomic displacements in the plane.

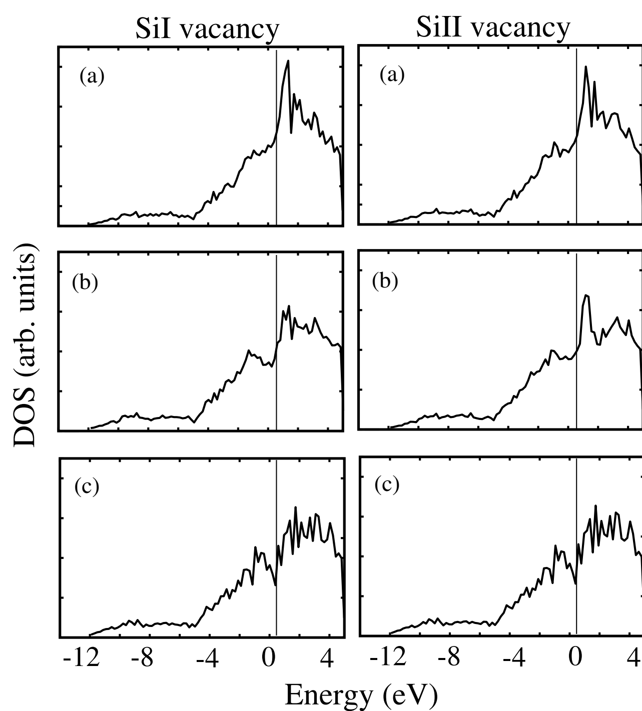

Figure 9. Electronic DOS projected onto the four Ti nearest neighbours of the Si I vacancy (left) and on the six Ti nearest neighbours of the Si II vacancy (right), in the C49 structure. (a) DOS computed as soon as the Si atom has been extracted. (b) DOS computed on the relaxed configuration, after the thermal annealing. (c) Reference DOS projected on the same set of atoms when no defect has been created in the equilibrated supercell.

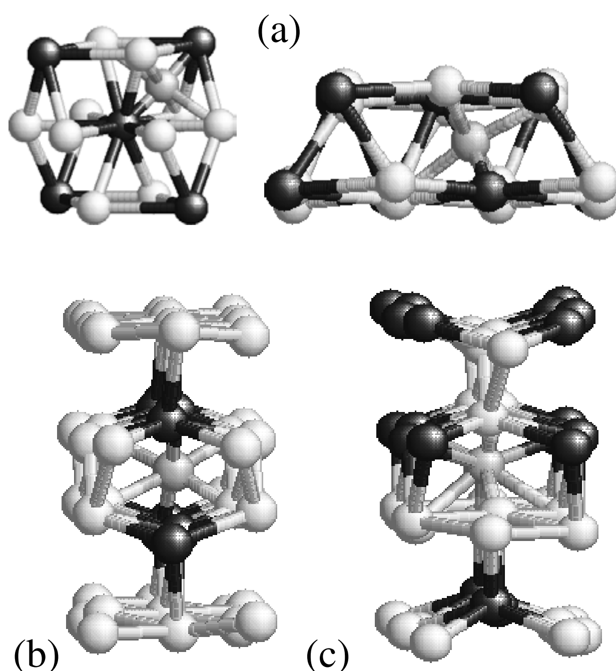

Figure 10. (a) Initial position of the Si interstitial (grey sphere) in the C54 structure (two different views are reported), and of two cases in the C49 structure, (b) and (c), see text.

4. Interstitials and defect pairs

Due to the close-packed structure of $TiSi_2$, interstitial point defects are not likely to be energetically favourable. Still, the formation energy of interstitials is an interesting probe of the structural properties of the C49 and C54 forms. In our case, we just consider the Si interstitials, which can be of some interest in Si diffusion during the solid state reaction (Si is expected to be the migrating species) [16, 19]. Moreover, the uncorrelated pair of interstitial and vacancy may be considered as the simplest example of defect pairs which do not require stoichiometric changes.

The $TiSi_2$ phases have quite a complex structure and no high symmetry interstitial sites can be easily identified. Therefore, we selected a few positions for each phase, which are suggested by the largest volume available (steric criterion), and by some preliminary calculations with a reduced number of atoms per simulation cell ($\sim$200). The most promising site for the close-packed and high symmetry C54 lattice was the interplanar region, between the (001) stoichiometric planes. Panel (a) in figure 10 reports one prototypical initial configuration, in two different views. The grey sphere is the interstitial Si atom, which has two Ti neighbours at about 1.6 Å and four Si neighbours at distances in the range 2.0–2.3 Å.

By contrast, the same procedure for the more open C49 lattice indicates at least two inequivalent low-energy sites. One is positioned in the region between the two Si II layers (shown in figure 10(b)); the second is between the Si I layer and the Ti layer (see panel (c) in the same figure). The interstitial represented in panel (b) is surrounded by two Ti neighbours, some 2 Å apart, and four Si II atoms located between 1.8 and 2.1 Å. In contrast, the interstitial site indicated in panel (c) has three Ti neighbours (at 1.9, 2.4 and 2.9 Å), four Si I neighbours in the range 1.9–2.7 Å and only one Si II neighbour at 1.5 Å.

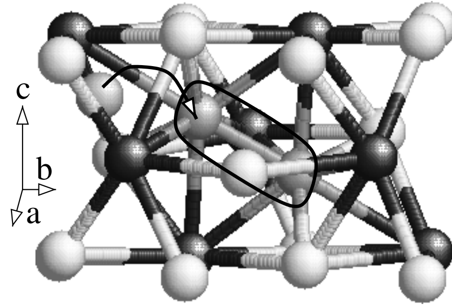

Figure 11. Selected atoms surrounding the interstitial Si atom (grey sphere) in the relaxed C54 cell. The arrow points out the path of the interstitial from the initial position, whereas the black curve encloses the two Si atoms in the dumbbell configuration at equilibrium.

By starting from these configurations, simulated annealing is performed at constant pressure and the defected structures are relaxed. The simulation cell contains 385 atoms in the three cases. The size guarantees convergence in energy, as we have already checked in the vacancy case.

The formation energy of the interstitial can be determined according to

$$E_f = E^{\mathbb{N}+Si} - E^{\mathbb{N}} - \xi_{tot}^{\mathrm{c-Si}} \tag{3}$$

where the first term on the right side is the equilibrium total energy of the defective cell, the second term is the reference value for the cell without defects and the last term is the Si site energy in the silicon substrate. We set the system free to rise in temperature because of the potential energy release due to the steric repulsion. The three samples (figures 10(a)–(c)) reached 640, 90 and 100 K, respectively. When the temperature was stabilized, we started cooling down the system by activating a velocity rescaling algorithm [20]. For the sake of comparison, after the first quench to 1 K the two C49 samples were heated up to 500 K and then cooled down again, with no sizeable changes.

After the quench to 1 K, the interstitial formation energy in the C54 structure, reported in table 3, displays the lowest value. A large decrease in total energy with respect to the first step is likely to be favoured by a new atomic arrangement which is a dumbbell configuration around the Si site. This is displayed in figure 11, where the dumbbell is circled by a solid line and the arrow points out the displacement of the extra Si atom, from its starting site to the relaxed position.

For the two C49 cases, interstitial formation energies can be considered nearly equivalent, even if the final atomic configurations are rather dissimilar. In the first case (b), the Si ends up in the stabilizing Ti–Si–Ti atomic configuration, as depicted in figure 12. The new Ti–Si–Ti configuration appears along the *c*-axis and allows for a partial saturation of the Ti d non-bonding states [21]. In contrast, the Si starting from the (c) configuration only gets closer to the Si I layer, but the formation energy is nearly the same as in case (b). Here again, a quantitative comparison to other similar systems with no substrate is difficult for the same reasons as outlined in the case of vacancies.

By considering the uncorrelated formation of a Si vacancy–interstitial pair (in the C49 form the vacancy is produced at the Si I site), we obtain the formation energy as

$$E_f = E^{\mathbb{N}+\mathrm{Si}} + E^{\mathbb{N}-\mathrm{Si}} - 2E^{\mathbb{N}}, \tag{4}$$

which are reported in table 4 for the corresponding interstitial positions of table 3. Here no quantitative problem arises in the determination of $\xi_{tot}^{\mathrm{c-Si}}$, and the formation energy for a defect

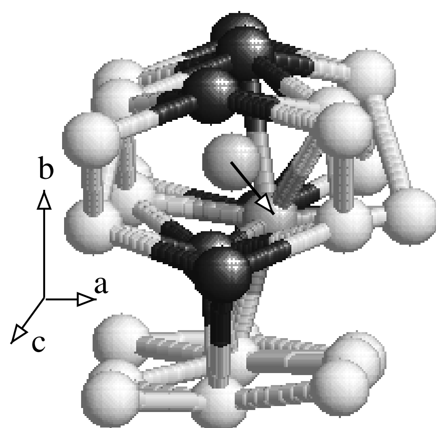

Figure 12. Selected atoms surrounding one Si interstitial (grey sphere) in the C49 case (case (b) of figure 10). In particular, the arrow indicates the displacement of the extra Si atom with relaxation, which ends up along a Ti chain.

Table 3. Interstitial formation energies relative to the samples containing 385 atoms. The estimates for the C49 structure, (b) and (c), correspond to two different interstitial positions (see text).

	E_f (eV)
C54(a)	2.34
C49(b)	3.18
C49(c)	3.27

Table 4. Formation energies for uncorrelated interstitial–vacancy pairs, where the two cases for the C49 structure (b), (c) correspond to the Si I vacancy and the two interstitial positions reported in table 3.

	E_f (eV)
C54(a)	5.05
C49(b)	3.65
C49(c)	3.74

pair in C54 $TiSi_2$, which is much larger than the one for the corresponding defect in C49 $TiSi_2$, is fully meaningful also in comparison to the single-crystal case.

We end this section by introducing some further evidence for the difference in the structural response of the two competitive phases, when an exchange in the Ti and Si sites is created. This is a useful tool to check how the surrounding atoms redistribute their bonding energy and rearrange the atomic environment. Each sample contains 288 atoms and has been studied after simulated annealing, at constant pressure. We investigate three exchange configurations in each phase, corresponding to different nearest-neighbour pairs [22]. The formation energies after the relaxation are displayed in table 5, where a conventional labelling I, II and III is used to indicate the pair exchange. Also in this case the defect pairs in the C54 form turn out to be more energy demanding because of the large recovery in the binding energy of the C49 phase. This is particularly true when a Si I site is involved (cases I and II). The analysis of the site energy distribution (reported in [22]) reveals that after the relaxation the perturbation in the C54 structure is still localized, whereas in the C49 case the excess energy is finally redistributed all over the simulation cell.

Table 5. Formation energies for 'pair exchanges', i.e. a double antisite. Each defected configuration is included in the supercell containing 288 atoms.

	Exchange Index	E_f (eV)
	I	3.95
C54	II	4.52
	III	4.21
	I	1.26
C49	II	1.35
	III	2.02

Table 6. Migration energy (E_m) and activation energy ($E_m + E_f$) for each type of point defect. The data related to the Si vacancy in the C49 phase refer to the Si I vacancy, because at high temperature the Si II vacancies turn into Si I ones.

	E_m (eV)	$E_m + E_f$ (eV)
C54 Si vacancy	0.72 ± 0.17	3.42
C49 Si I vacancy	0.83 ± 0.35	1.32
C54 Si interstitial	1.0 ± 0.2	3.34
C49 Si interstitial	1.4 ± 0.6	4.62

5. Diffusion coefficients for point defects

In a previous work [21] we made a preliminary investigation on the diffusion phenomena in the C54 and C49 phases. In particular, the mobility of silicon atoms has been observed at high temperature for the two competing phases. The main focus was set on the diffusion by defects (Si interstitial and Si vacancy) and the corresponding diffusivities were extracted in terms of the mean square displacements, by

$$d(T) = \lim_{t\to\infty} \frac{1}{6t} \sum_{i}^{N} [\vec{r}_i(t) - \vec{r}_i(0)]^2 = d_0 \exp[-E_m/k_B T], \tag{5}$$

where t is the simulation time, N is the number of atoms, $\vec{r}_i(t)$ is the position of the ith atom at t and $\vec{r}_i(0)$ is its starting position. This form is equivalent to the exponential definition where the migration energy E_m appears. However, in [19] the formation energy of vacancies and interstitials was evaluated without accounting for the role of the Si substrate, as in the present work. Thereby, by combining the new formation energies reported here and the migration energies estimated in [21] we get the activation energies ($E_f + E_m$) for the diffusion coefficient

$$D(T) = d(T)X_v = d_0 \exp[-(E_m + E_f)/k_B T]. \tag{6}$$

The results are reported in table 6. We may claim that the most efficient diffusion mechanism is confirmed to be the vacancy diffusion in the C49 phase. This is determined by the very low formation energy of Si I vacancies and by the preferential diffusion of Si by Si I vacancies in the Si I (010) plane. However, the migration energy of Si in the C54 form appears to be slightly lower, probably due to the most efficient hopping between Si nearest neighbours, as produced by the largest coordination of equivalent sites (see table 1).

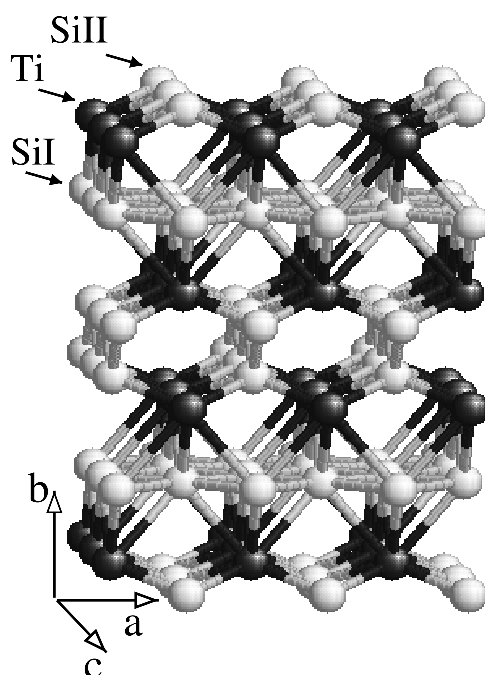

Figure 13. C49 supercell, as obtained by multiplying the conventional orthorhombic cell by three along $\boldsymbol{a}$, two along $\boldsymbol{b}$, and three along $\boldsymbol{c}$. The atomic layers are stacked along [010] in the sequence Si II–Ti–Si I–Ti–Si II–Si II–Ti–Si I–Ti–Si II.

6. Stacking faults

One peculiar property of the C49 phase, as reported by some experimental observations [8, 23], is the high density of SFs along the [010] lattice direction. However, the actual structure of these SFs is still matter of discussion: what is commonly believed is that the poor conductivity of the C49 phase is very likely generated by such extended defects [11]. This is the reason why we focus our attention on the C49 structure.

One conventional orthorhombic cell of the C49 lattice can be constructed by two blocks of five atomic layers (Si II–Ti–Si I–Ti–Si II), stacked along the [010] direction. They are shifted one with respect to the other by $\boldsymbol{a}/2$ in between adjacent Si II planes (see figure 13). Still, due to the nearly equal size of $\boldsymbol{a}$ and $\boldsymbol{c}$ sides, at least two other stackings are possible, which generate slightly different structures, with no changes in the coordination at nearest neighbours. In particular, if the second block is shifted by $\boldsymbol{c}/2$ in place of $\boldsymbol{a}/2$, a SF characterized by the shift vector $\frac{1}{2}(\boldsymbol{a}+\boldsymbol{c})$ is obtained, as already described in the literature [23]. One other possible configuration is obtained by rotating the second block by 90° along the $\boldsymbol{b}$ axis and shifting it by $\frac{1}{4}(\boldsymbol{a}+\boldsymbol{c})$. Therefore, SFs are more likely to occur between two adjacent Si II (010) planes in the C49 structure. However, for the sake of comparison, we test also one SF created between the Ti layer and the Si I layer, by the 'usual' SF vector $\frac{1}{2}(\boldsymbol{a}+\boldsymbol{c})$. Hereafter the faulted configurations described above are named SFA, SFB and SFC, respectively.

In order to simulate the faulted structure (including the one with a 90° rotation along $\boldsymbol{b}$, SFB), we initially set $a = c = 3.61$ Å (average between the a and c experimental values [12]), so that the slightly rectangular pattern parallel to (010) turns into a square one. The faulted

Table 7. Formation energy, cell sides and volume per atom measured after the numerical annealing of the faulted C49 cells SFA, SFB and SFC. The cell sides of the simulation cell in bulk configuration, equilibrated by our potential, are $a = 14.22$ Å, $b = 26.80$ Å, $c = 15.01$ Å (see footnote 6).

	E_f	Cell sides (Å)			Volume
Configuration	(eV Å^{-2})	$\tilde{a}$	$\tilde{b}$	$\tilde{c}$	(Å^3/atom)
SFA	3.99×10^{-3}	14.82	26.35	14.77	15.02
SFB	4.28×10^{-3}	14.19	26.68	15.03	14.81
SFC	8.92×10^{-3}	15.41	25.20	15.05	15.22

samples are constituted by a cell containing 384 atoms, $\tilde{a} = 4a$, $\tilde{b} = 2b$, $\tilde{c} = 4c$. Due to periodic boundary conditions along $\boldsymbol{b}$, each simulation cell contains two SFs, separated by ~13.5 Å. The most straightforward way to verify the long-range modification in this faulted structure is the analysis of the differences between the C49 ideal lattice (as tetragonalized by setting $a = c$) and the faulted configurations, by the differential plots of the pair distribution functions and of the angular distributions within 4 Å (figure 14). First, we note that the differences in the partial pair distributions function, $g(r)$, always appear beyond $r = 4$ Å, and this means that there are no effects on the nearest neighbours. The SFA and SFB cases do not generate variations in the Ti–Ti pairs up to 6 Å, at variance with the SFC case. As concerns the Ti–Si and Si–Si pairs the SFA configuration bears a larger perturbation than the SFB.

In the pair distribution functions no changes are visible below 4 Å, but some distortions of the bonds between the nearest neighbours can be pointed out in the angular distribution, $P(\theta)$. The related panels in figure 14 display the differential angular distributions computed by choosing the Ti site as centre and considering the Si–Ti–Si angles within 4 Å. The differential $P(\theta)$ for the SFA shows the same features, twice as large, as the SFB one. Actually, no changes are present in the Ti–Ti–Ti, Ti–Si–Ti and Si–Si–Si angular distributions, when either the SFA and SFB configurations are considered (some slight variations appear in the case of SFC).

Starting from these configurations, which are expected to require a modest energy increase, we perform structural relaxation by MD simulations by heating to 200 K (2 ps) and hold at constant temperature for 2 ps more. Finally, we quench the temperature to 1 K in 5 ps, with a constant cooling rate of 4×10^{13} K s^{-1}. Actually, one interesting feature to look at is the final size of $\tilde{\boldsymbol{a}}$ and $\tilde{\boldsymbol{c}}$ sides, since they might remain slightly different, as suggested by the original orthorhombic symmetry, or tetragonalize (i.e. $a = c$), as indicated by recent x-ray diffraction measurements, and by *ab initio* relaxations for a cell size much smaller than the ones we consider here [10].

In table 7 the SF formation energies E_{SF} are displayed, as calculated by

$$E_{SF} = \frac{E - E_0}{A_{SF}}, \tag{7}$$

where E is the total energy of the faulted cell, E_0 is the total energy of the original cell containing the same number of atoms (384) and A_{SF} is the total SF area at equilibrium. Our estimations of the formation energies are of the same order as the ones recorded for silicon ($E_f = 5.0 \times 10^{-3}$ eV Å^{-2}), reported by Antonelli *et al* [24]. We conclude that all the three SF formation energies are rather low, in particular SFA and SFB.

We note that the SFB cell takes almost the same shape and volume as the one for bulk C49 phase, reported in the caption of table 7. Hence, the initial tetragonalization ($a = c$) is lost and the initial volume per atom decreases to 14.81 Å^3. The volume per atom of the SFA cell increases to 15.02 Å^3, and the a and c sides are still almost equal in size. As concerns the b side, it assumes almost the same value as the one characterizing the bulk C49 structure in both

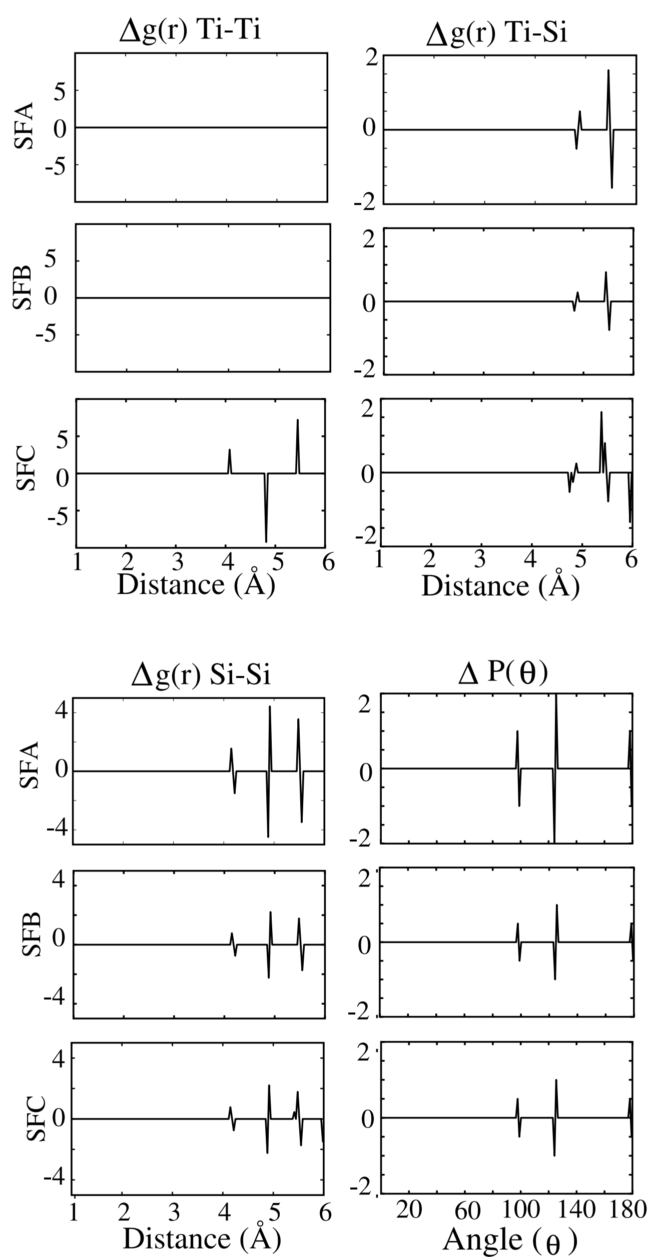

Figure 14. Differential pair distribution functions $\Delta g(r)$ (Ti–Ti, Ti–Si and Si–Si) and angular distribution functions $\Delta P(\theta)$ (Si–Ti–Si within 4 Å), computed for the faulted cells with respect to the ideal one: the top panels refer to SFA, the middle ones to SFB and the bottom ones to SFC (see text).

the SFA and SFB cases. In contrast, the *b*side in SFC is rather short. Such arguments, along with the trend in the formation energies, support the idea that only SFA and SFB configurations are likely to occur in the C49 structure.

Acknowledgment

This work was partially supported by CNR grant nos CT88.00042.PF30 and 97.01355.PS48.

Appendix

Within the TB model the estimation of the '*covalent*' energy of the ith site is given by

$$\xi^i = \sum_n f_n \varepsilon_n \sum_\alpha |C_{i\alpha}^{(n)}|^2, \tag{8}$$

where n runs over the eigenvalues of the Hamiltonian matrix (ε_n), f_n is the occupation of the nth state, α are the atomic orbitals $C_{i\alpha}^{(n)}$ are the components of the nth eigenvector relative to the ith atom. ξ^i, in turn, is composed by two terms. The first is the bond-energy contribution which is the strength of pair interactions i–j,

$$\xi_{bond}^i = \sum_{j\neq i} \sum_n f_n \sum_{\alpha\beta} C_{j\beta}^{*(n)} H_{i\alpha j\beta} C_{i\alpha}^{(n)}, \tag{9}$$

where $H_{i\alpha j\beta}$ are the off-diagonal elements of the Hamiltonian matrix, providing the interaction between the α orbital of the ith atom and the β orbital of the jth atom.

The second is the *onsite* energy

$$\xi_{onsite}^i = \sum_n f_n \sum_\alpha C_{i\alpha}^{*(n)} H_{i\alpha i\alpha} C_{i\alpha}^{(n)}, \tag{10}$$

which refers to the occupation inside the crystal. The total site energy, ξ_{tot}^i, is then obtained by adding to ξ^i the repulsive contribution ξ_{rep}^i, as computed by the phenomenological two-body potential, described in our previous work [1].

References

[1] Iannuzzi M, Celino M and Miglio L 2000 *Phys. Rev.* B **61** 14 450
[2] Colgan E G, Gambino J P and Hong Q Z 1996 *Mater. Sci. Eng.* **R16** 2
[3] Beyers R and Sinclair R 1985 *J. Appl. Phys.* **57** 5240
[4] Dehm C, Gyulai J and Ryssel H 1992 *Appl. Phys. Lett.* **60** 1214
[5] Beyers R, Coulman D and Merchant P 1987 *J. Appl. Phys.* **61** 5110
[6] Nemanich R J, Fulks R T, Stafford B L and Vander Plas H A 1985 *Appl. Phys. Lett.* **46** 670
Nemanich R J, Fulks R T, Stafford B L and Vander Plas H A 1985 *J. Vac. Sci. Technol.* A **3** 938
Nemanich R J, Doland C M, Fulks R T and Ponce F A 1986 *Mater. Res. Soc. Symp. Proc.* **54** 255
[7] Jeon H, Sukow C A, Honeycutt J W, Rozgonyi G A and Nemanich R J 1992 *J. Appl. Phys.* **71** 4269
[8] Chou T C, Wong C Y and Tu K N 1987 *J. Appl. Phys.* **62** 2275
[9] Migas D B, Iannuzzi M, Miglio L, La Via F and Grimaldi M G 1999 *Mater. Res. Soc. Symp. Proc.* **580**
[10] La Via F, Grimaldi M G, Migas D B and Miglio L 2001 *Appl. Phys. Lett.* **78** 739
[11] Mattheiss L F 1989 *Phys. Rev.* B **39** 7754
[12] Villars P (ed) 1997 *Pearson's Handbook of Crystallographic Data for Intermetallic Phases* (Materials Park, Ohio: American Society for Metals)
[13] Rosenkranz R and Frommeyer G 1992 *Z. Metall.* **83** 9
[14] Lide D R (ed) 1997 *Handbook of Chemistry and Physics* 78th edn, ed C Bernard (Boca Raton, FL: Chemical Rubber Company Press)
Bernard C (Institut National Polytechnique de Grenoble) private communication
[15] Chou M Y and Mercer J L 1993 *Phys. Rev.* B **47** 9366
Koyama M 1991 *J. Phys.: Condens. Matter* **3** 2193
Kwon *et al* 1994 *Phys. Rev.* B **49** 7242
Lenosky T J *et al* 1997 *Phys. Rev.* B **55** 1528
[16] Gas P, Scilla G, Michel A, Le Goues F K, Thomas O and d'Heurle F M 1988 *J. Appl. Phys.* **63** 5335
[17] Wang B Y, Wang Y X, Gu Q and Wang T M 1997 *Comput. Mater. Sci.* **8** 267
[18] Kummerle E A, Badura K, Sepiol B, Mehrer H and Schaefer H E 1995 *Phys. Rev.* B **52** R6947

[19] Iannuzzi M, Raiteri P, Celino M and Miglio L 2001 *J. Comput. Mater. Sci.* **20** 394
[20] Allen M P and Tildesley D J 1987 *Computer Simulation of Liquids* (Oxford: Clarendon)
[21] Miglio L, Iannuzzi M, Raiteri P and Celino M 2001 *Microelectron. Eng.* **55** 83
[22] Iannuzzi M 2000 Kinetic advantages of the C49 $TiSi_2$ over the C54 phase by thermodynamic analysis via tight binding molecular dynamics *PhD Thesis* University of Milano-Bicocca
[23] Ma Z and Allen L H 1995 *J. Appl. Phys.* **71** 4384
[24] Antonelli A, Justo J F and Fazzio A 1999 *Phys. Rev.* B **60** 4711